Steel and Composite Structures, *Vol. 30, No. 4 (2019) 315-325*
DOI: https://doi.org/10.12989/scs.2019.30.4.315

Height-thickness ratio on axial behavior of composite wall with truss connector

Ying Qin [1a], Gan-Ping Shu [*1], Xiong-Liang Zhou [2], Jian-Hong Han [1] and Yun-Fei He [2]

[1] *Key Laboratory of Concrete and Prestressed Concrete Structures of Ministry of Education, and National Prestress Engineering Research Center, School of Civil Engineering, Southeast University, Nanjing, China*
[2] *Zhejiang Southeast Space Frame Group Company Limited, Hangzhou, China*

(*Received November 4, 2018, Revised February 12, 2019, Accepted February 14, 2019*)

Abstract. Double skin composite walls offer structural and economic merits over conventional reinforced concrete counterparts in terms of higher capacity, greater stiffness, and better ductility. This paper investigated the axial behavior of double skin composite walls with steel truss connectors. Full-scaled tests were conducted on three specimens with different height-to-thickness ratios. Test results were evaluated in terms of failure mode, load-axial displacement response, buckling loading, axial stiffness, ductility, strength index, load-lateral deflection, and strain distribution. The test data were compared with AISC 360 and Eurocode 4 and it was found that both codes provided conservative predictions on the safe side.

Keywords: axial behavior; composite wall; truss connector; height-to-thickness ratio; structural performance

1. Introduction

Thin steel plates are vulnerable to local buckling, which may be distributed through the whole structure and result in global collapse (Mirtaheri and Zoghi 2016, Zoghi and Mirtaheri 2016). Therefore, the early local buckling of steel plate should be prevented in practical design. Buckling-restrained brace, as the component to resist lateral load, is effective in preventing the buckling in compression through the encasing of steel core into a steel tube and confining concrete infill (Gheidi *et al*. 2011, Mirtaheri *et al*. 2018). Similarly, concrete-filled tube column prevents the buckling of steel tube by the infilled concrete (Qin *et al*. 2015a, b, 2016, 2018a).

Double skin composite wall is another effective component to restrain the buckling of steel plate. It comprises of vertically aligned flat steel faceplates and infilled concrete core and has been applied to safety-related facilities such as gravity seawalls, floating breakwater, submerged tube tunnels, nuclear containment, ship hulls and protective structures (Huang and Liew 2016). The steel faceplates are relatively thin and vulnerable to local buckling, while the infilled concrete core offers restraint against buckling (Qin *et al*. 2017a, 2018b, c). Therefore, the double skin composite wall with appropriate design can be considered as ductile system.

The double skin composite walls provide structural and economic merits over conventional reinforced concrete counterparts in terms of higher capacity, greater stiffness, and better ductility (Sakr *et al*. 2017, Korkmaz and Ecemis 2017). The steel faceplates act as the permanent formwork for casting concrete during the construction stage, which improves construction efficiency and reduces the on-site labor cost and time. Furthermore, the steel faceplates on the external sides provide waterproof characteristics which makes it convenient for maintenance and inspection. The inherent features of easy pre-fabrication in factories and rapid installation on site further promote the efficiency in time and reduce the cost. During the service stage, the steel faceplates can work together with the infilled concrete core to serve as the composite wall to carry axial loading.

The composite action between steel faceplates and concrete core is achieved by employing appropriate type of load transfer devices in the form of embossments or other internal mechanical connectors (Hilo *et al*. 2016, Shekastehband *et al*. 2018). Various mechanical connectors have been proposed by former researchers to lock the two materials together, such as headed studs (Luo *et al*. 2015, Yan *et al*. 2018), tie bars (Ji *et al*. 2017), embedded cold-formed steel tubes (Hilo *et al*. 2016), J-hook connectors (Huang and Liew 2016), ring stiffened tubes (Liao and Ma 2018), and combined transverse stiffeners, vertical diaphragms and distributed batten plates (Huang *et al*. 2018).

An innovative double skin composite wall system with steel truss connector has been developed as shown in Fig. 1. The trusses which consists of kinked rebar and angles, are directly fillet welded to the inner surface of steel faceplates by automatic machine. Concrete is filled between the steel faceplates to form the composite walls. This type of connector is believed to offer good performance because of its high pull out strength.

Most of the previous studies on double skin composite walls have focused on the seismic behavior under cyclic loading (Eom *et al*. 2009, Nie *et al*. 2014, Luo *et al*. 2015, Nguyen and Whittaker 2017, Yousefi and Ghalehnovi 2018), while some research has been conducted on the axial behavior (Choi *et al*. 2014, Huang and Liew 2016, Qin *et*

*Corresponding author, Professor,
E-mail: shuganping@seu.edu.cn
[a] Associate Professor, E-mail: qinying@seu.edu.cn

ISSN: 1229-9367 (Print), 1598-6233 (Online)

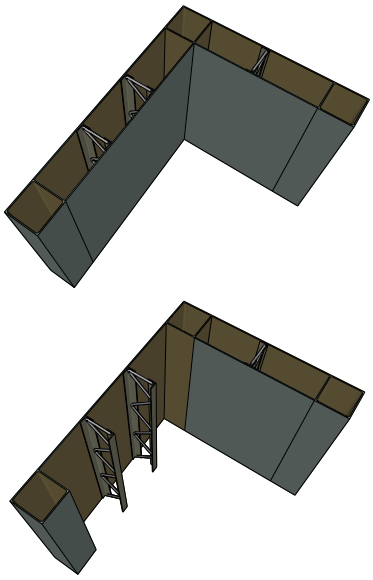

Fig. 1 Composite wall with steel truss as connector

al. 2017b). However, the primary objective of these studies was to investigate the compressive resistance of short walls with small height-to-width ratio, whose failure modes were governed by cross-sectional capacity. There is a dearth of information on tall walls with high height-to-width ratio whose failure may be controlled by global buckling.

This research investigated the axial behavior of composite walls with steel trusses connectors. Full-scaled compressive tests were performed on three specimens with different height-to-thickness ratios. The structural response of the proposed walls was evaluated in details, and the influences of height-to-thickness ratio were comprehensively discussed. Development of detailed finite element and analytical models to simulate the compressive behavior of this type of wall will be discussed in a companion paper.

2. Experimental program

2.1 Test specimen

Three innovative double skin composite walls, labelled as SCW-150, SCW-180, and SCW-200, were tested under axial compressive loading. The variable in the research is the thickness of the wall, which is denoted by the numbers of 150, 180, and 200 in millimetre. The corresponding height-to-thickness ratios for three specimens are 20, 16.7, and 15, respectively. The specimens were designed and fabricated at the full scale to investigate the actual structural behaviour of this type of walls. The detailed configurations of the test specimens are illustrated in Fig. 2 and Table 1. All test specimens have identical cross-sectional dimensions and steel truss configurations except for the thickness of the walls. The cross-sectional dimensions of the test specimens were 3000 mm in height and 1500 mm in width, including the concrete-filled square tubular columns located at two sides of the cross section to serve as the boundary elements. The dimensions of the concrete-filled tubular columns are

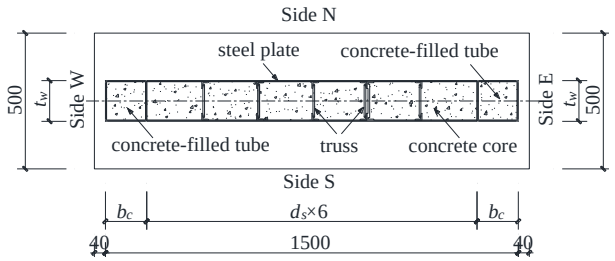

Fig. 2 Specimen details

Table 1 Specimen details

Specimen No.	h_w	b_w	t_w	t_s	d_s	$b_c \times t_c$
	mm	mm	mm	mm	mm	mm×mm
SCW-150	3000	1500	150	4	200	150×4
SCW-180	3000	1500	180	4	200	150×4
SCW-200	3000	1500	200	4	200	150×4

*Note: h_w, b_w and t_w are the height, width and thickness of test walls; t_s is the thickness of steel faceplate; d_s is the spacing of steel truss; b_c is the width of concrete-filled tubular column along the direction of wall width; and t_c is the thickness of tubular column

150 × 150 × 4 mm, 150 × 180 × 4 mm, 150 × 200 × 4 mm,respectively, for Specimens SCW-150, SCW-180, and SCW-200. The differences in dimensions of columns correspond to the different wall thicknesses. The thickness of steel faceplates is 4 mm. The steel truss is composed of two angles with the dimension of 40 × 40 × 4 mm and rebar with the diameter of 8 mm. The spacing of the steel truss is 200 mm, which is determined by limiting the width-to-thickness ratio of stiffened steel faceplate. The requirement for the width-to-thickness ratio should be less than $60\sqrt{235/f_y}$ according to Technical specification for steel plate shear walls (JGJ/T 380-2015 2015). The wall is attached to a base plate and a top plate for convenience in installation and loading in the reaction frame.

2.2 Material properties

The strength grade of the infilled concrete core of all specimens is C20 whose characteristic value of cubic strength is 20 MPa, according to the Chinese code for design of concrete structures (GB20010-2010 2010). Six cubes with the dimension of 150 × 150 × 150 mm were cast to obtain the actual cubic compressive strength. The tested average value of cubic compressive strength is 23.5 MPa.

The strength grade of the steel faceplates and tubular columns is Q235 with nominal yield strength of 235 MPa, based on the Chinese standard for classification of steel structures (GB50017-2017 2017). Four coupons were prepared to obtain the actual material properties. The tested average yield strength, ultimate strength, modulus of elasticity, and elongation were 261.6 MPa, 362.8 MPa, 2.05 × 10^5 MPa, and 31%, respectively, for tubular columns, and 346.0 MPa, 364.8 MPa, 1.99 × 10^5 MPa, and 34%, respectively, for steel faceplates.

Fig. 3 Test setup

2.3 Test setup and loading procedure

The double skin composite walls were tested in the 20,000 kN multi-functional loading reaction frame, as shown in Fig. 3. The base of the specimen was clamped onto the reaction frame by high-strength bolts, while the top of the specimen was connected to a spreader beam with sufficient stiffness. Lateral braces were provided to prevent the lateral displacement of spreader beam. The axial compressive force was applied to the specimen by two hydraulic actuators with the individual capacity of 10,000 kN. The force control method with the load interval of 363.64 kN was used to apply the compression. Each loading level was maintained until the deformation and the strain had been fully developed.

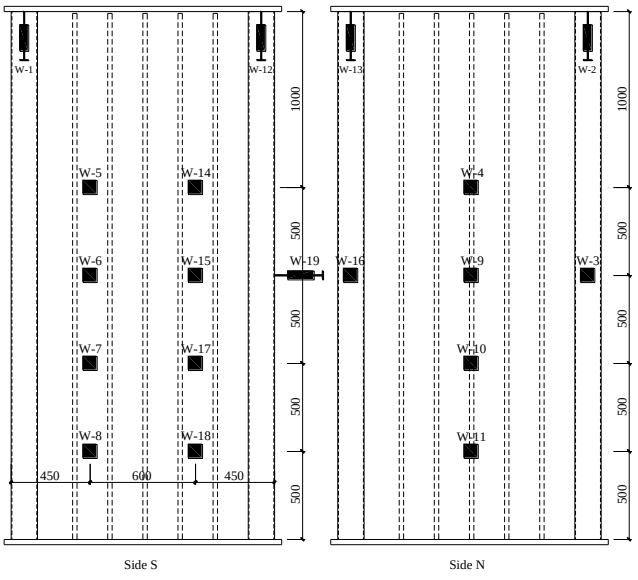

Fig. 4 Arrangement of displacement transducers

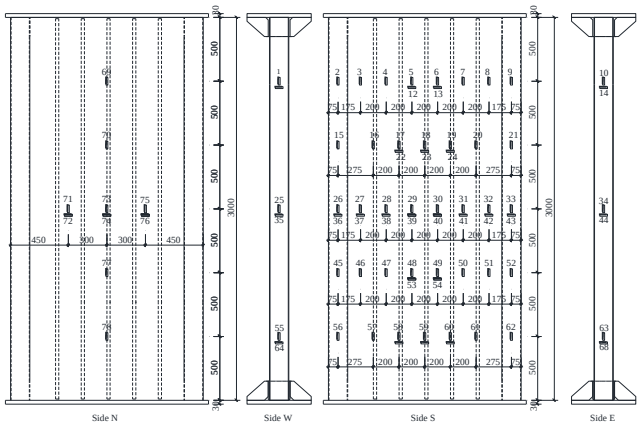

Fig. 5 Arrangement of strain gauges

2.4 Instrumentations

Figs. 4 and 5 show the arrangement of linear variable differential transducers (LVDTs) and strain gauges, respectively. LVDTs W1, W2, W12, W13 were placed at the top of specimen to monitor the axial displacement during the test. Fifteen horizontal LVDTs (W3-W11, W14-W19) were installed along the height of the wall to measure the lateral displacement at different heights. Strain gauges were arranged on the surface of the wall to monitor the strain development of the concrete-filled tube columns and steel faceplates.

3. Axial compression test

3.1 General observation

Specimen SCW-150 exhibited elastic behavior and no local buckling of steel faceplates could be found at the beginning of the test. As the axial load arrived at 4000 kN, small sounds were emitted from the specimen, which implied that the buckling started to develop. During the loading level of 5455 kN, slight buckling was observed on the steel faceplates on side N at the height of 500 mm from the base. When the axial load came to 6545 kN, the steel faceplate on side S at the height of about 200 mm from the top reached its buckling strain. The specimen reached its peak load of 8182 kN at the axial displacement of 17.28 mm. After the peak load, the specimen experienced global buckling as shown in Fig. 6(a). In addition, the buckling of steel faceplate became more seriously and rapidly on side S as shown in Fig. 6(b) and extended to the area of 450 mm from the top of the wall, as can be seen from Fig. 6(c). The failure photograph of Specimen SCW-150 is shown in Fig. 6(d).

The structural behavior of Specimen SCW-180 was similar to that of Specimen SCW-150. No obvious deformation or damage was observed until the loading level of 6909 kN. As the axial load arrrived at 6909 kN, slight buckling was observed at the lower half height of wall on side N. The buckling became more severe as the load progressed. When the load reached 9455 kN, clear sound

(a) Global buckling

(b) Buckling on side S

(c) Buckling on side N

(d) Failure of specimen

Fig. 6 Test observation of Specimen SCW-150

was emitted from the specimen and the concrete-filled tubular column on side E bulged outwards at the top. As the specimen reached its peak load of 9818 kN, global buckling occurred as shown in Fig. 7(a). Steel faceplates on both sides N and S buckled at the middle height of the wall, as shown in Figs. 7(b) and (c), respectively. Meanwhile, slight buckling was observed at the bottom of the concrete-filled tubular column, as shown in Fig. 7(d).

For Specimen SCW-200, steel faceplace slightly buckled at the distance of 1200 mm from the top of wall on side S at the load level of 5455 kN. As the load progressed to 7273 kN, the buckling extended to the area of 750 mm from the top of wall. At the loading level of 7636 kN, buckling occurred on side N at the height of 1000 mm from the base. Similar buckling waves were found on side N at the heigth of 1000 mm from the top of wall. Meanwhile, steel faceplate severely buckled on side S at a distance of 200 mm from the top. When the axial load reached 8727

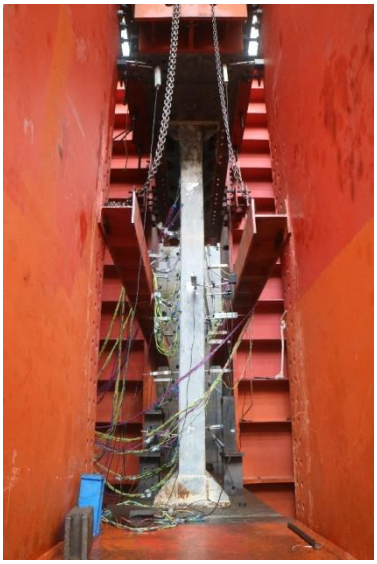

(a) Global buckling

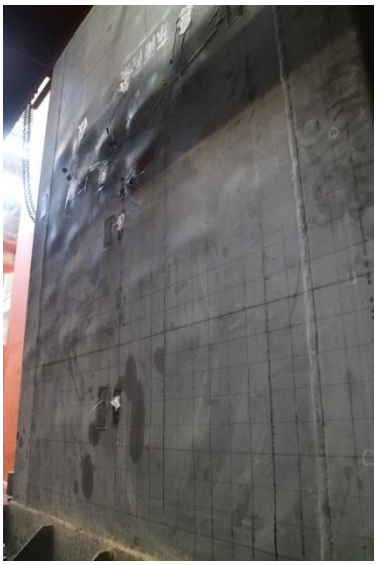

(b) Buckling on side N

Fig. 7 Test observation of Specimen SCW-180

(c) Buckling on side S

(d) Buckling of boundary column

Fig. 7 Continued

kN, buckling could be seen at the top of concrete-filled tubular column. At the loading level of 9091 kN, big sound was heard and the axial shortening was obvious. The peak load was achieved at the level of 10182 kN. After the peak load, the buckling of steel faceplates became more serious, accompanied with obvious crushing of infilled concrete

(a) Severe buckling on side S

Fig. 8 Test observation of Specimen SCW-200

(b) Severe buckling on side N

(c) Failure mode

Fig. 8 Test observation of Specimen SCW-200

(Figs. 8(a) and (b)), which led to deterioration of its axial compressive resistance. The failure of Specimen SCSW-200 is shown in Fig. 8(c).

3.2 Failure modes

As can be seen from the test observation, there are two types of failure modes observed from the test. The first type of failure mode is local buckling occurring in steel faceplates, followed by the global buckling of the wall. Specimens SCW-150 with the height-to-thickness ratio of 20 and SCW-180 with the height-to-thickness ratio of 16.7 fail in this type of mode. The second type of failure is the cross-sectional capacity failure. This type of failure is observed in Specimen SCW-200 with the height-to-thickness ratio of 15.

4. Experimental results

4.1 Load-axial displacement response

Fig. 9 shows the axial load versus axial displacement curves for all specimens under compression. The load-axial displacement response is closely linear before the local buckling of steel faceplates. When the steel faceplates start to buckle, the specimens entered the inelastic stage, together with slight deterioration of strength and stiffness. After that,

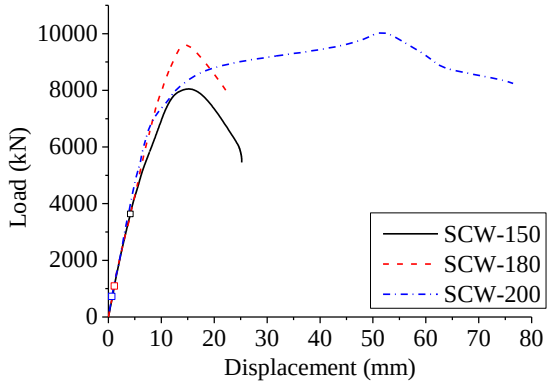

Fig. 9 Load-axial displacement curves

the axial resistance of the specimens arrived at the maximum capacity. During the post-peak stage, the axial resistance of the wall began to decline as a result of overall instability or severe crush of concrete. Obvious deterioration of strength and stiffness could be observed in this stage, in which Specimen SCW-200 exhibits the most favarable strength and stiffness deterioration.

4.2 Buckling stress

When the double skin composite walls are loaded under axial compression, the steel truss connectors can be considered as the boundary edges for steel faceplates and thus, the steel faceplates tend to buckle between the two adjacent steel trusses. Furthermore, due to the presence of infilled concrete core, the steel faceplates can only buckle along the outward rather than the inward direction. As can be seen from Figs. 6-8, the steel faceplates buckle horizontally with half-waves. Strain gauges were used to measure the strain development of steel faceplates under each loading level.

When buckling occurs on steel faceplate, the strain changes rapidly due to the local bending of the steel faceplate. The buckling stress σ_b and the corresponding buckling load N_b can then be determined from the inflection points of the load-strain curves.

Fig. 10 plots the partially-enlarged drawings of load-strain curves of three specimens. The inflection points are labelled by red squares in the curves. As can be seen from Fig. 10(a), Specimen SCW-150 has a buckling strain of -736×10^{-6} $\mu\varepsilon$, and the corresponding buckling stress and buckling load are 146.5 Mpa and 3636 kN, respectively. The curves from Fig. 10(b) shows that Specimen SCW-180 has a buckling strain of -246×10^{-6} $\mu\varepsilon$, and the corresponding buckling stress and buckling load are 49.0 Mpa and 1091 kN, respectively. Based on the strain curves in Fig. 10(c), Specimen SCW-200 has a buckling strain of -153×10^{-6} $\mu\varepsilon$, and the corresponding buckling stress and buckling load are 30.4 Mpa and 727 kN, respectively. It can be observed that the ratios of the buckling stress to the yield stress for Specimens SCW-150, SCW-180, and SCW-200 are 0.42, 0.14, and 0.09, respectively. This indicates that the steel truss in specimen with greater height-to-thickness ratio owns larger stiffness to resist the possible tensile force caused by the buckling of steel faceplate.

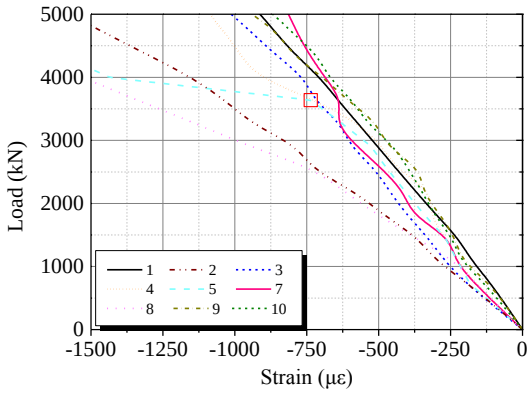

(a) Specimen SCW-150

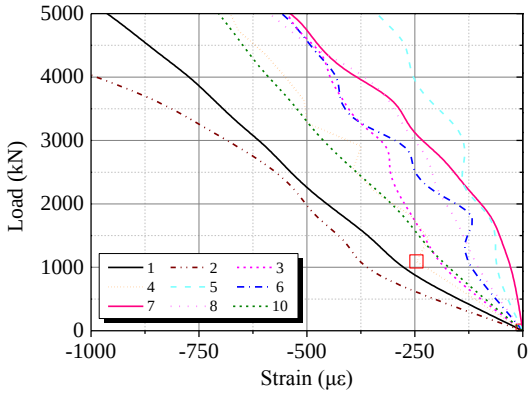

(b) Specimen SCW-180

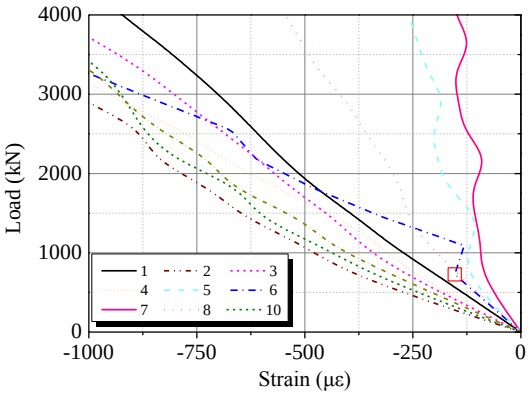

(c) Specimen SCW-200

Fig. 10 Partially-enlarged drawing of strain curves

Euler theory offers equations to predict the elastic buckling stress σ_{cr} of double skin composite walls as shown in Eq. (1).

$$\sigma_{cr} = \frac{\pi^2 E_s}{12k^2 \left(d_s / t_s\right)^2} \tag{1}$$

where k is the effective length factor; d_s is the spacing between trusses; and t_s is the thickness of steel faceplate.

The results of the test specimens, together with the available data in literature publication (Akiyama and Sekimoto 1991, Usami *et al*. 1995, Kanchi 1996, Choi and Han 2009) are plotted in Fig. 11 in terms of the relationship between the normalized buckling strain $\varepsilon_{cr}/\varepsilon_y$ and the

normalized slenderness ratio $d_s/t_s \times \sqrt{f_y/E_s}$. The red dash line and the blue solid line represent the Euler curves with k = 0.7 and k = 1.0, respectively. It can be found that the data of Specimen SCW-150 lies between the two Euler curves, while the data of Specimens SCW-180 and SCW-200 are below the curve with k = 1.0. This indicates that the thicker walls provide less restraint to the outwards buckling of steel faceplate and leads to a more flexible boundary condition. This is because for steel truss with the identical dimension of angles and rebar, increasing the spacing between the two angles may possibly reduce the stiffness of the truss, and results in the fact that the steel truss provides weaker support.

4.3 Axial stiffness

Table 2 gives the buckling load N_b and the corresponding displacement Δ_b, peak load N_u and the corresponding displacement Δ_u, $0.3N_u$ and the corresponding displacement $\Delta_{0.3u}$, $0.6N_u$ and the corresponding displacement $\Delta_{0.6u}$. The buckling loads are also labelled in Fig. 9 by squares. It can be seen from Fig. 9 that no apparent change in stiffness can be observed after the local buckling of steel faceplates. This means the influence of buckling on axial stiffness is not significant.

In order to quantify the effect of buckling on axial stiffness, two types of secant stiffness are employed. The first (k_b) uses the buckling load point as the starting point and the $0.6N_u$ point as the terminal point, while the second ($k_{0.3u}$) uses the $0.3N_u$ point as the starting point and the $0.6N_u$ point as the terminal point. The two methods generate similar values of stiffness as given in Table 2. It can be observed that the two methods generate similar results, which indicates that the axial stiffness of double skin composite wall does not significantly decrease after the buckling of steel faceplate. In addition, the secant axial stiffness increases with the decrease in height-to-thickness ratio. This is expected as larger cross-sectional area results in larger axial stiffness.

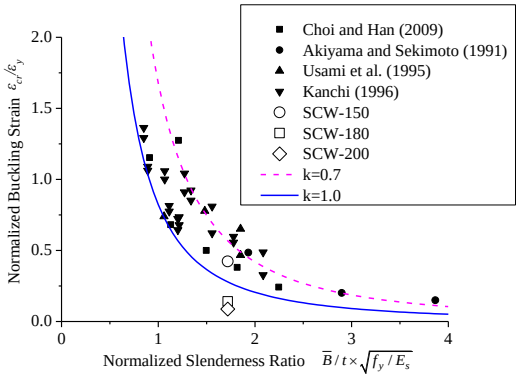

Fig. 11 Comparison with Euler curves

4.4 Ductility

Ductility ratio (μ) is used to quantify the ability of the walls to develop significant plastic deformation without noticeable strength deterioration. It can be defined as the ratio of the nominal maximum axial displacement (Δ_m) to the yield axial displacement (Δ_y), where the nominal maximum axial displacement Δ_m is the displacement corresponding to $0.85N_u$ during the descending stage; and the yield axial displacement Δ_y is determined by the universal yield–bending–moment method (Xiong *et al.* 2017).

The yielding load N_y and the corresponding displacement Δ_y, the nominal maximum load $0.85N_u$ and the corresponding displacement Δ_m, and the ductility ratio μ are listed in Table 3. It can be observed that Specimen SCW-200 has the largest ductility ratio of 4.63, while the ductility ratios for Specimens SCW-150 and SCW-180 are 1.91 and 1.70, respectively. The great differences in ductility ratio are due to the different failure modes. The failure of Specimen SCW-200 is caused by the capacity failure, and the deformation had been fully developed, while the failure of the other two specimens is caused by overall instability, which leads to the rapid degradation of strength after the peak load. This also demonstrates that the ductility is significantly affected by the height-to-thickness ratio.

4.5 Strength index

Strength index (*SI*) is used to evaluate the capacity utilization of double skin composite walls and can be calculated by Eq. (2). The calculated values of *SI* for three specimens are given in Table 3. The values of *SI* for Specimens SCW-180 and SCW-200 are greater than one

Table 3 Ductility and strength index

Specimen No.	N_u	Δ_y	$0.85N_u$	Δ_m	μ	*SI*
	kN	mm	kN	mm		
SCW-150	7490	11.25	6955	21.53	1.91	0.98
SCW-180	9050	12.33	8345	20.96	1.70	1.06
SCW-200	8260	14.31	8655	66.22	4.63	1.03

Table 2 Stiffness calculation

Specimen No.	N_b	Δ_b	N_u	Δ_u	$\frac{N_b}{N_u}$	$0.3N_u$	$\Delta_{0.3u}$	$0.6N_u$	$\Delta_{0.6u}$	K_b	$K_{0.3u}$	$\frac{K_{0.3u}}{K_b}$
	kN	mm	kN	mm		kN	mm	kN	mm	kN/mm	kN/mm	
SCW-150	3636	4.15	8182	17.28	0.44	2455	2.63	4909	6.04	674	720	1.07
SCW-180	1091	1.14	9818	14.91	0.11	2945	3.26	5891	6.90	833	809	0.97
SCW-200	727	0.65	10182	51.61	0.07	3055	3.13	6109	6.82	872	828	0.95

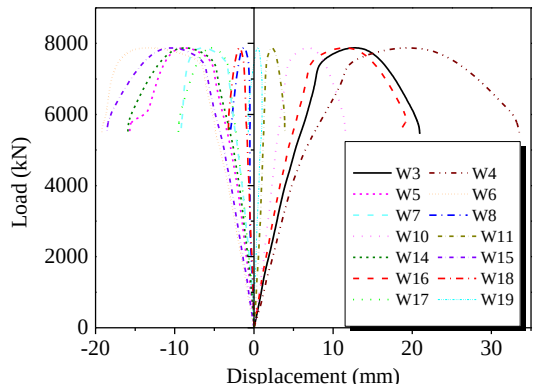

(a) Specimen SCW-150

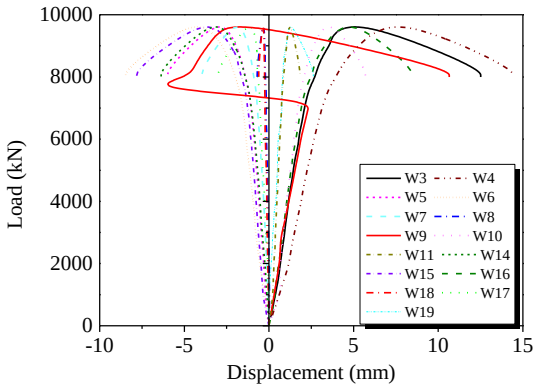

(b) Specimen SCW-180

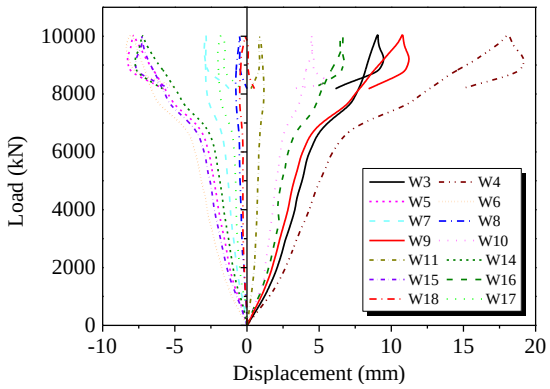

(c) Specimen SCW-200

Fig. 12 load-lateral deflection curves

due to the fact that the contribution of steel trusses is excluded in the calculation of fully-utilized capacity.

$$SI = \frac{N_u}{N_0} \tag{2}$$

$$N_0 = f_y A_s + f_c' A_c \tag{3}$$

where N_u is the ultimate capacity obtained from the test; N_0 is the fully-utilized capacity of the cross-section and can be calculated by Eq. (3); f_y and f'_c are the yield strength of steel and compressive strength of concrete core, respectively; A_s and A_c are the cross-sectional area of steel and concrete core, respectively.

4.6 Load-lateral deflection response

Figs. 12(a)-(c) give the load-lateral deflection curves for three specimens. It can be seen that the largest lateral deflection under each loading level occurs mostly at the middle height of the wall. The deflection slowly and linearly grows up as the axial load increases at the beginning of the loading. The slope of the curves rapidly changes when the specimens are approaching their peak load. After that, the deflection continues to increase as the load starts to go down. Furthermore, the in-plane lateral deflection is quite small, as can be seen from the value of displacement transducer W19.

4.7 Load-strain relationship

The load-strain response for Specimen SCW-180 is shown in Fig. 13. The load-strain relationships of the other two specimens are similar and thus, they are not presented herein.

The longitudinal strains along the vertical direction behave in a linear increase at the beginning of the loading until the steel buckles. The longitudinal strains rapidly grow after reaching the peak load. Furthermore, under each loading level, the strains develop more quickly at a distance closer to the loading point. This indicates that part of axial force on the steel faceplates is transferred to the concrete core through steel truss connectors.

The strains in the same row are more uniform at the locations where the steel trusses are located, which means the steel trusses do contribute to the more uniform distribution of axial force.

4.8 Code-base design

The compressive strength of composite walls in AISC 360-16 (2016) can be determined by Eqs. (4)-(5).

$$\text{When } \frac{P_{no}}{P_e} \le 2.25, \quad N_{AISC} = P_{no}\left(0.658^{\frac{P_{no}}{P_e}}\right) \tag{4}$$

$$\text{When } \frac{P_{no}}{P_e} > 2.25, \quad N_{AISC} = 0.877 P_e \tag{5}$$

where $P_{no} = f_y A_s + f_{yt} A_{st} + 0.85 f_c' A_c$; $P_e = \frac{\pi^2 EI_{eff}}{L_c^2}$ is the elastic critical buckling load; and readers could refer to AISC 360-16 (2016) for the definition of other parameters.

The compressive strength of composite wall in Eurocode 4 (EN 1994-1-1:2004 2004) is determined by Eq. (6).

$$N_{EC4} = \chi N_{pl,Rd} \tag{6}$$

where $N_{pl,Rd} = f_{st} A_{st} + f_s A_s + 0.85 f_c' A_c$; and readers could refer to Eurocode 4 (EN 1994-1-1:2004 2004) for the definition of other parameters.

Table 4 gives the predictions by AISC 360-16 (2016) and EN 1994-1-1:2004 (2004). It can be observed that the predictions by the two codes are close. The average ratio and standard deviation of test results to predictions are 1.20

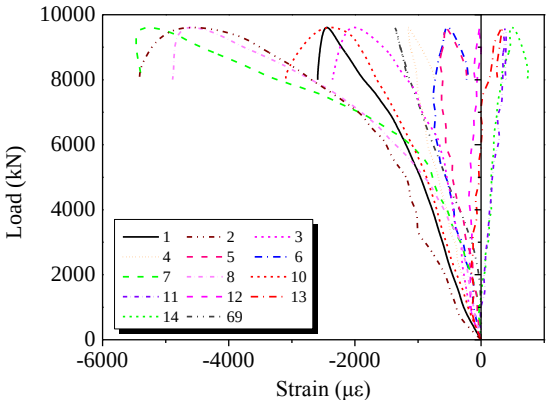

(a) The 1st row

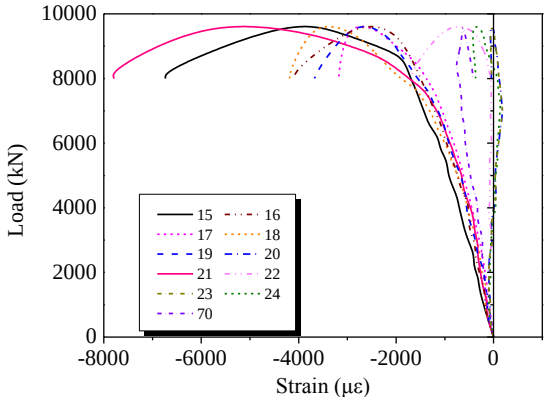

(b) The 2nd row

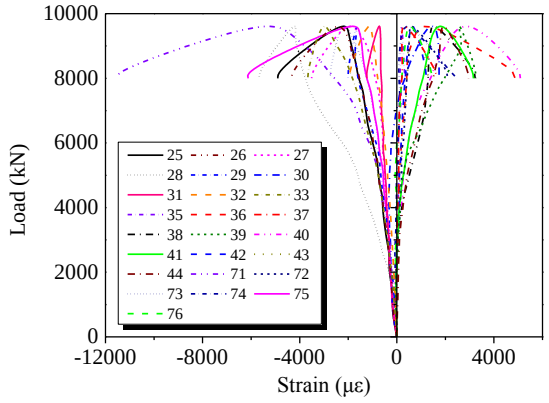

(c) The 3rd row

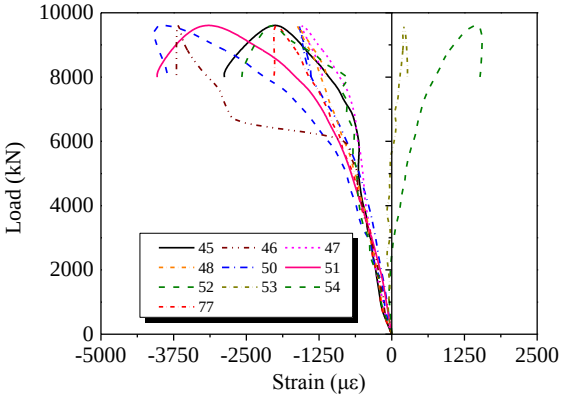

(d) The 4th row

Fig. 13 Load-strain curves for Specimen SCW-180

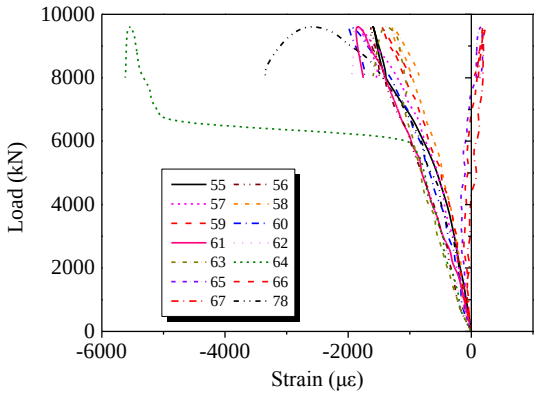

(e) The 5th row

Fig. 13 Continued

Table 4 Comparison with code-based prediction

Specimen No.	N_u	N_{AISC}	$\frac{N_u}{N_{AISC}}$	N_{EC4}	$\frac{N_u}{N_{EC4}}$
	kN	mm	kN	mm	
SCW-150	8182	7165	1.14	7057	1.16
SCW-180	9818	7934	1.24	7894	1.24
SCW-200	10182	8428	1.21	8438	1.21
Average			1.20		1.20
Standard deviation			0.040		0.035

and 0.040, respectively, for AISC, while those are 1.20 and 0.035, respectively, for Eurocode 4. Two codes both offer conservative predictions, which is on the safe side.

5. Conclusions

In this paper, the compressive behavior of double skin composite walls with steel truss connectors was investigated. Axial compression tests were performed on three full-scaled specimens with different height-to-thickness ratios. The conclusions are drawn as below:

(1) Two failure modes are identified in the test. One is the local buckling of steel faceplates and the sequent global buckling of the wall, while the other is the cross-sectional capacity failure. In practical design, for composite walls with height-to-thickness ratio less than 15, the strength failure may dominate, while for composite walls with height-to-thickness ratio greater than 15, the global buckling should be considered in design equation.

(2) For walls with given height and width, the reduction in height-to-thickness ratio may change the failure mode. Furthermore, it leads to the growth in axial stiffness and the decrease in buckling load. Meanwhile, the effects of height-to-thickness ratio on ductility and strength index are not significant.

(3) Both AISC 360 and Eurocode 4 provide

conservative predictions for the load-bearing capacity of double skin composite walls on the safe side.

Acknowledgments

This work is sponsored by the Natural Science Foundation of Jiangsu Province (Grant No. BK20170685), the National Key Research and Development Program of China (Grant No. 2017YFC0703802), the National Natural Science Foundation of China (Grant No. 51808117), the Jiangsu Overseas Visiting Scholar Program for University Prominent Young & Middle-aged Teachers and Presidents, and the Fundamental Research Funds for the Central Universities (Grant No. 2242018K40137). The authors would like to thank the Zhejiang Southeast Space Frame Group Company Limited for the supply of test specimens, and Hui-Kai Zhang, Xin Yan, Ke-Rong Luo, Shi Cao, and Rui Pan in the steel research group of Southeast University for their assistance with the laboratory work.

References

AISC 360-16 (2016), Specification for structural steel buildings; American Institute of Steel Construction, Chicago, IL, USA.

Akiyama, H. and Sekimoto, H. (1991), "A compression and shear loading tests of concrete filled steel bearing wall", *Transaction of 11th Structural Mechanics in Reactor Technology* (SMiRT-11), Tokyo, Japan, August.

Choi, B.J. and Han, H.S. (2009), "An experiment on compressive profile of the unstiffened steel plate-concrete structures under compression loading", *Steel Compos. Struct., Int. J.*, **9**(6), 519-534.

Choi, B.J., Kang, C.K. and Park, H.Y. (2014), "Strength and behavior of steel plate–concrete wall structures using ordinary and eco-oriented cement concrete under axial compression", *Thin Wall. Struct.*, **84**, 313-324.

EN 1994-1-1:2004 (2004), Eurocode 4: Design of composite steeel and concrete structures-Part 1-1: General rules and rules for buildings; British Standards Institution, London, UK.

Eom, T.S., Park, H.G., Lee, C.H., Kim, J.H. and Chang, I.H. (2009), "Behavior of double skin composite wall subjected to in-plane cyclic loading", *J. Struct. Eng.*, **135**(10), 1239-1249.

GB50010-2010 (2010), Code for design of concrete structures; China Architecture & Building Press, Beijing, China.

GB50017-2017 (2017), Standard for classification of steel structures; China Architecture & Building Press, Beijing, China.

Gheidi, A., Mirtaheri, M., Zandi, A.P. and Alanjari, P. (2011), "Effect of filler material on local and global behaviour of buckling-restrained braces", *Struct. Des. Tall Spec. Build.*, **20**(6), 700-710.

Hilo, S.J., Badaruzzaman, W.H.W., Osman, S.A. and Al-Zand, A.W. (2016), "Structural behavior of composite wall systems strengthened with embedded cold-formed steel tube", *Thin Wall. Struct.*, **98**, 607-616.

Huang, Z.Y. and Liew, J.Y. (2016), "Compressive resistance of steel-concrete-steel sandwich composite walls with J-hook connectors", *J. Constr. Steel Res.*, **124**, 142-162.

Huang, S.T., Huang, Y.S., He, A., Tang, X.L., Chen, Q.J., Liu, X.P. and Cai, J. (2018), "Experimental study on seismic behaviour of an innovative composite shear wall", *J. Constr. Steel Res.*, **148**, 165-179.

JGJ/T 380-2015 (2015), Technical specification for steel plate shear walls; China Architecture & Building Press, Beijing, China.

Ji, X.D., Cheng, X.W., Jia, X.F. and Varma, A.H. (2017), "Cyclic in-plane shear behavior of double-skin composite walls in high-rise buildings", *J. Struct. Eng.*, **143**(6), 04017025.

Kanchi, M. (1996), "Experimental study on a concrete filled steel structure Part 2 Compressive tests (1). Summary of Technical Papers of Annual Meeting", Architectural Institute of Japan, 1996, 1071-1072.

Korkmaz, H.H. and Ecemis, A.S. (2017), "Seismic upgrading of reinforced concrete frames with steel plate shear walls", *Earthq. Struct., Int. J.*, **13**(5), 473-484.

Liao, J.J. and Ma, G.W. (2018), "Energy absorption of the ring stiffened tubes and the application in blast wall design", *Struct. Eng. Mech., Int. J.*, **66**(6), 713-727.

Luo, Y.F., Guo, X.N., Li, J., Xiong, Z., Meng, L., Dong, N.C. and Zhang, J. (2015), "Experimental research on seismic behaviour of the concrete-filled double-steel-plate composite wall", *Adv. Struct. Eng.*, **18**(11), 1845-1858.

Mirtaheri, M. and Zoghi, M.A. (2016), "Design guides to resist progressive collapse for steel structures", *Steel Compos. Struct., Int. J.*, **20**(2), 357-378.

Mirtaheri, M., Sehat, S. and Nazeryan, M. (2018), "Improving the behavior of buckling restrained braces through obtaining optimum steel core length", *Struct. Eng. Mech., Int. J.*, **65**(4), 401-408.

Nguyen, N.H. and Whittaker, A.S. (2017), "Numerical modelling of steel-plate concrete composite shear walls", *Eng. Struct.*, **150**, 1-11.

Nie, J.G., Ma, X.W., Tao, M.X., Fan, J.S. and Bu, F.M. (2014), "Effective stiffness of composite shear wall with double plates and filled concrete", *J. Constr. Steel Res.*, **99**, 140-148.

Qin, Y., Chen, Z.H. and Rong, B. (2015a), "Component-based mechanical models for concrete-filled RHS connections with diaphragms under bending moment", *Adv. Struct. Eng.*, **18**(8), 1241-1255.

Qin, Y., Chen, Z.H. and Rong, B. (2015b), "Modeling of CFRT through-diaphragm connections with H-beams subjected to axial load", *J. Contr. Steel Res.*, **114**, 146-156.

Qin, Y., Chen, Z.H., Bai, J.J. and Li, Z.L. (2016), "Test of extended thick-walled through-diaphragm connection to thick-walled CFT column", *Steel Compos. Struct., Int. J.*, **20**(1), 1-20.

Qin, Y., Lu, J.Y. and Cao, S. (2017a), "Theoretical study on local buckling of steel plate in concrete filled tube column under axial compression", *ISIJ Int.*, **57**(9), 1645-1651.

Qin, Y., Shu, G.P., Fan, S.G., Lu, J.Y., Cao, S. and Han, J.H. (2017b), "Strength of double skin steel-concrete composite walls", *Int. J. Steel Struct.*, **17**(2), 535-541.

Qin, Y., Zhang, J.C., Shi, P., Chen, Y.F., Xu, Y.H. and Shi, Z.Z. (2018a), "Behavior of improved through-diaphragm connection to square tubular column under tensile loading", *Struct. Eng. Mech., Int. J.*, **68**(4), 475-483.

Qin, Y., Shu, G.P., Du, E.F. and Lu, R.H. (2018b), "Buckling analysis of elastically-restrained steel plates under eccentric compression", *Steel Compos. Struct., Int. J.*, **29**(3), 379-389.

Qin, Y., Du, E.F., Li, Y.W. and Zhang, J.C. (2018c), "Local buckling of steel plates in composite structures under combined bending and compression", *ISIJ Int.*, **58**(11), 2133-2141.

Sakr, M.A., El-Khoriby, S.R., Khalifa, T.M. and Nagib, M.T. (2017), "Modeling of RC shear walls strengthened by FRP composites", *Struct. Eng. Mech., Int. J.*, **61**(3), 407-417.

Shekastehband, B., Mohammadbagheri, S. and Taromi, A. (2018), "Seismic behavior of stiffened concrete-filled double-skin tubular columns", *Steel Compos. Struct., Int. J.*, **27**(5), 577-598.

Usami, S., Akiyama, H., Narikawa, M., Hara, K., Takeuchi, M. and Sasaki, N. (1995), "Study on a concrete filled steel structure for nuclear plants (part 2). Compressive loading tests on wall

members", *Transaction of 13th Structural Mechanics in Reactor Technology* (SMiRT-13), Porto Alegre, Brazil, August.
Xiong, Q.Q., Chen, Z.H., Zhang, W., Du, Y.S., Zhou, T. and Kang, J.F. (2017), "Compressive behaviour and design of L-shaped columns fabricated using concrete-filled steel tubes", *Eng. Struct.*, **152**, 758-770.
Yan, J.B., Wang, Z., Wang, T. and Wang, X.T. (2018), "Shear and tensile behaviors of headed stud connectors in double skin composite shear wall", *Steel Compos. Struct., Int. J.*, **26**(6), 759-769.
Yousefi, M. and Ghalehnovi, M. (2018), "Finite element model for interlayer behavior of double skin steel-concrete-steel sandwich structure with corrugated-strip shear connectors", *Steel Compos. Struct., Int. J.*, **27**(1), 123-133.
Zoghi, M.A. and Mirtaheri, M. (2016), "Progressive collapse analysis of steel building considering effects of infill panels", *Struct. Eng. Mech., Int. J.*, **59**(1), 59-82.

CC